25th anniversary of the Konus-Wind experiment 9-13 September 2019

Hard X-rays of Solar Flares, Acceleration and Electron Transport in Magnetoactive Plasma

Yu.E.Charikov, A.N.Shabalin, V.P.Ovchinnikova, V.I.Globina and I.D.Oparin

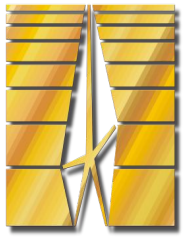

Ioffe Institute

POLYTECH
Peter the Great St.Petersburg Polytechnic University

Central Problems of Solar Flare Physics

1.The problem of flare energy storage

2. The problem of particle acceleration, transport and radiation in plasma magnetic loops

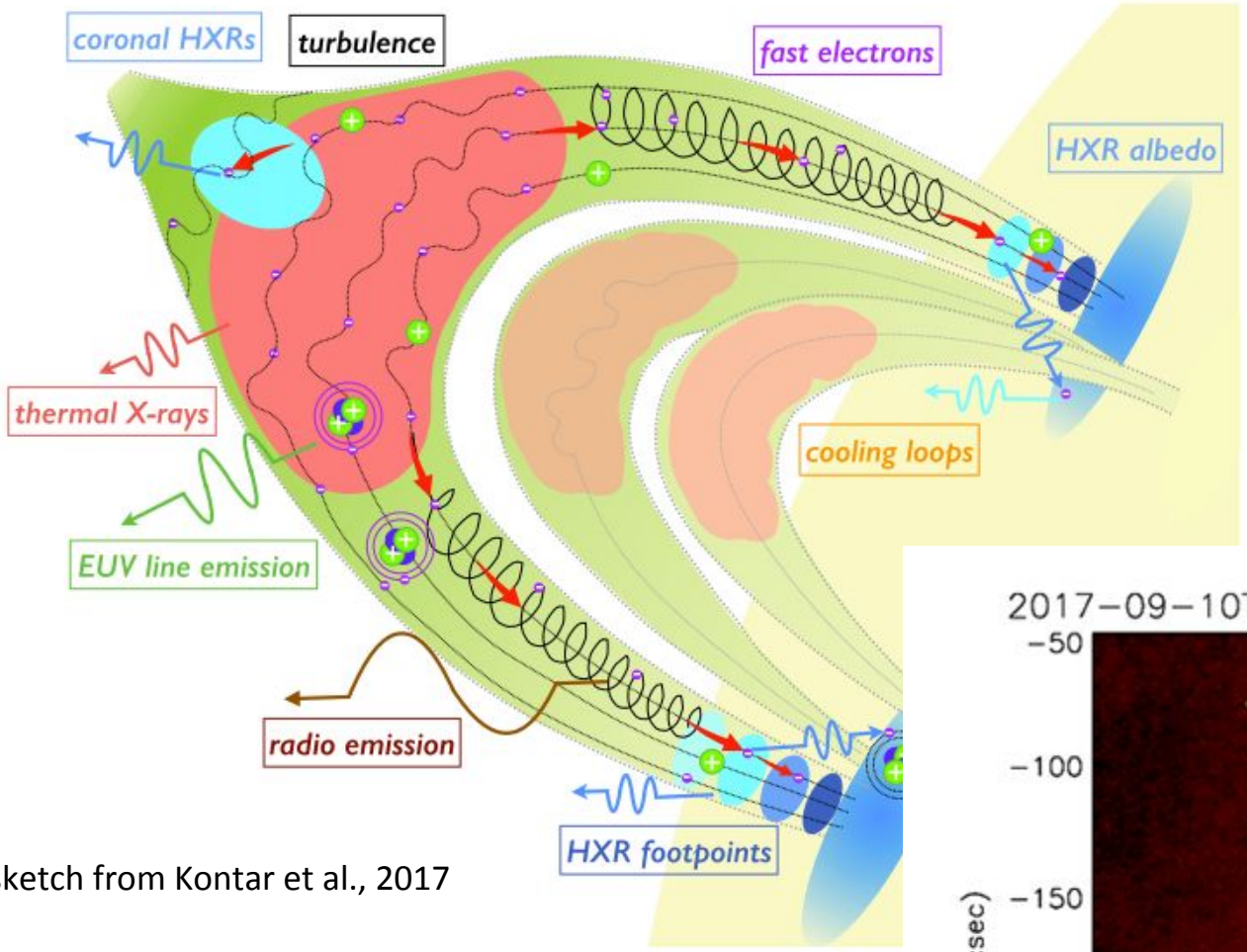

sketch from Kontar et al., 2017

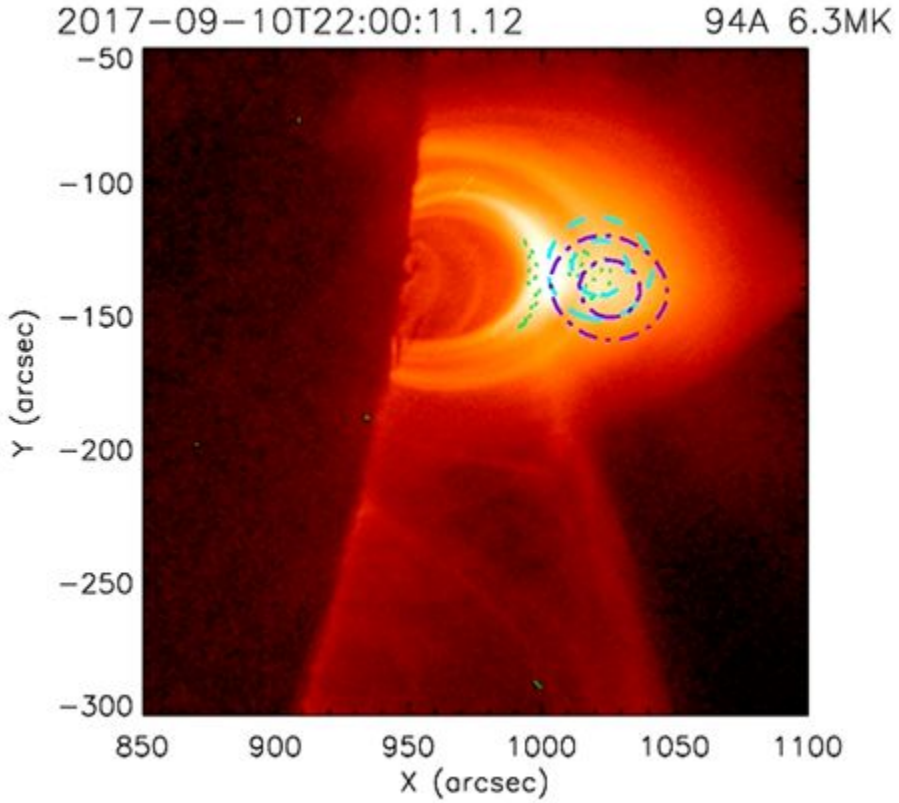

GX Simulator **SOL2002:11:10 T 03:11**, M2.6

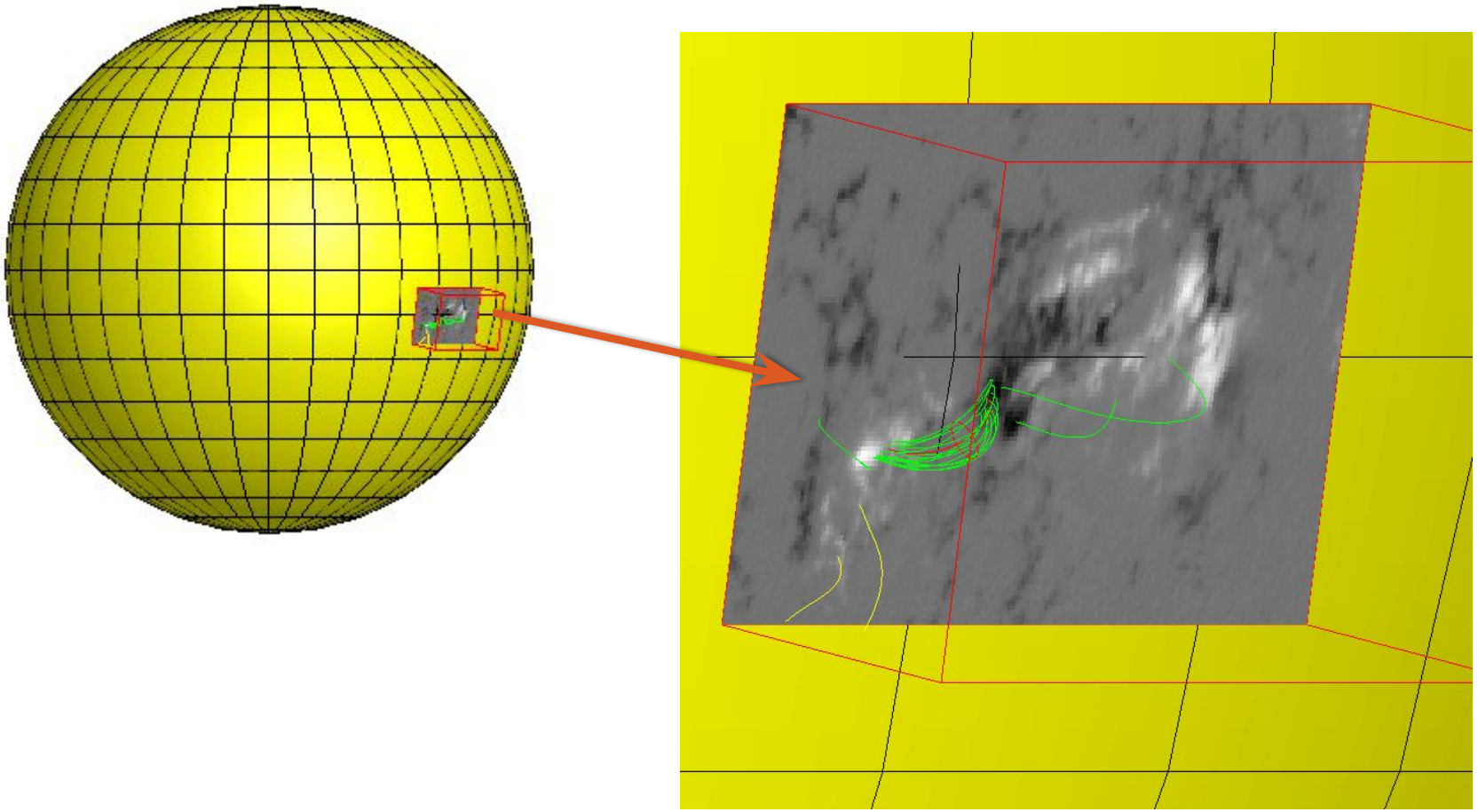

Nita et al, 2014

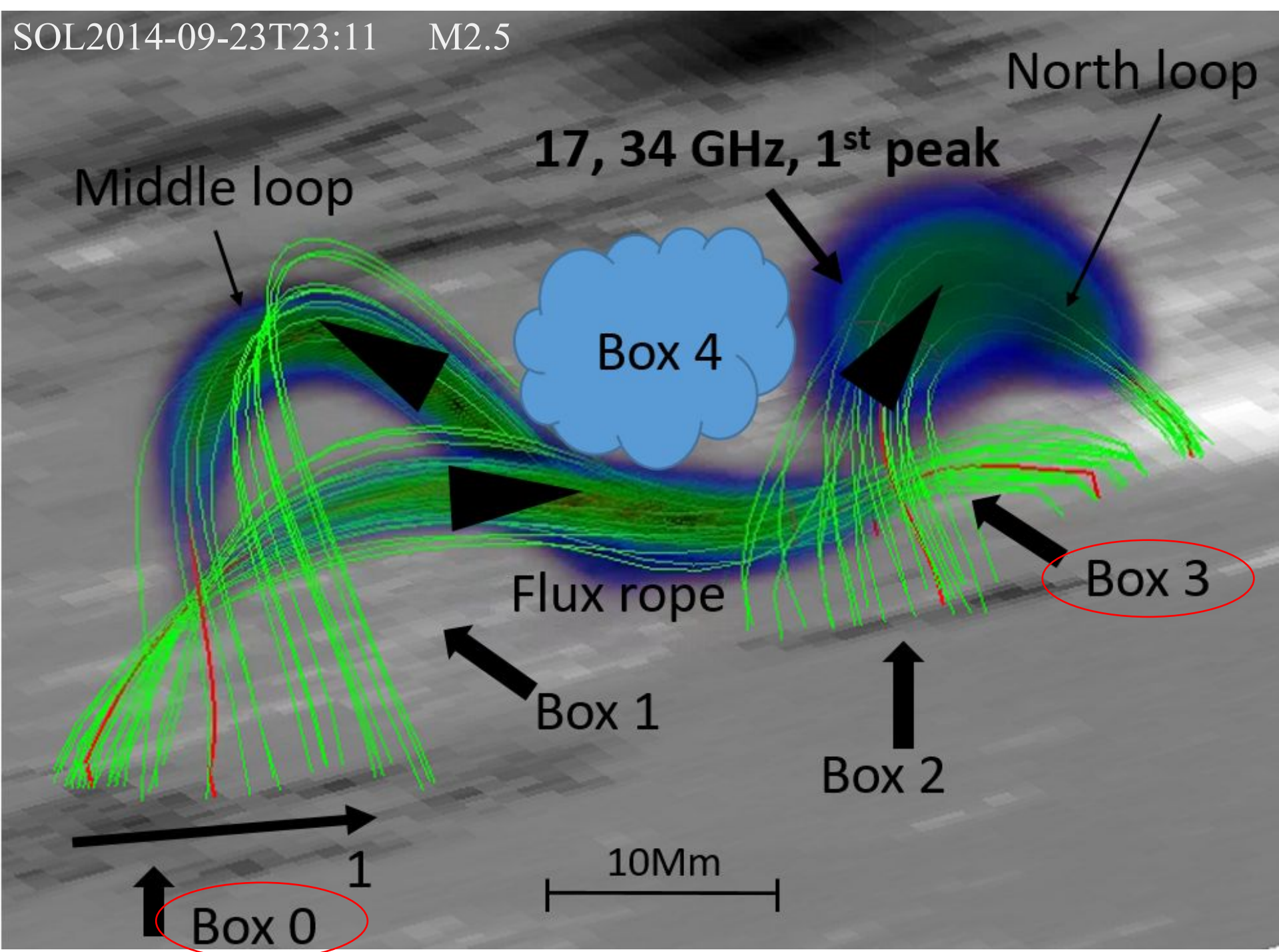
SOL2014-09-23T23:11 M2.5
North loop
17, 34 GHz, 1st peak
Middle loop
Box 4
Flux rope
Box 3
Box 1
Box 2
1
Box 0
10Mm

There are basically two faces of a solar flare — one concerns energetic particles and their transport and radiation effects, and the other concerns the hydrodynamic evolution of the plasma in the flare loop. These two aspects are actually coupled together in a circular chain. Particles, on the one hand, lose their energy via Coulomb collisions and heat the background plasma, which causes chromospheric evaporation that changes the density and temperature distribution in the loop. In turn, such changes affect the particle acceleration and transport processes and influence the spectrum of the accelerated particles. The energy deposition rate (by particles) will also be altered and fed back to the hydrodynamics of the background plasma.

Due to the complexity of the subject, however, people tend to decouple these processes and study one at a time while assuming some simple forms for the others. For particle acceleration and transport, as mentioned earlier, one of the main streams of studies solves the Fokker-Planck equation and keeps track of the particle distribution function (e.g., Leach 1984; McTiernan 1989), assuming a static background atmosphere.

Problem of Electron Transport

1. Restore the distribution function of accelerated electrons at the time of injection into the plasma of the magnetic loop.
2. Plasma and magnetic field diagnostics

To develop a method for determining the characteristics of background plasma (plasma density, temperature) and accelerated electrons (spectrum, localization, pitch-angular distribution) in flares based on observations of X-ray and microwave radiation.
In general, the kinetic equation with different initial electron distributions and plasma parameters is solved numerically and the influence of different processes on the beam and radiation dynamics is revealed.

Space and ground-based observations:

- Soft X-rays: **GOES** (1-8Å (1.5-12 keV), 0.5-4Å (3.1 – 24.8 keV)), **RHESSI** (3keV-20MeV)
- HXR: **RHESSI**, **Konus-Wind** (~20keV-20MeV), **BATSE** (20keV-1.9MeV), (**Fermi**)
- GS radiation: **NORH** (17, 34 GHz), **NORP** (1, 2, 3.75, 9, 17, 35, 80 GHz), (**EOVSA**, **CCPT**)
- UV image: **AIA**/SDO (9 lines 1700-94Å / 5000K-20MK), (**EIT**/SOHO)
- Magnetic field structure: **HMI**/SDO, **MDI**/SOHO

Software:

- Fokker-Planck kinetic code
- e-i, e-e bremsstrahlung of relativistic electrons:energy spectra, polarization degree, directivity
- Albedo calculation code
- SOLAR SOFT: GX Simulator (NLFFF/LFFF), HESSI, OSPEX, AIA, etc

Parameters affect the solar flare HXR and GS radiation

	Parameter	HXR >25 keV	GS (3-35GHz)
SDO/HMI SOHO/MDI	Angle of view, θ	+	+
	Magnetic field, B(s,t)	+ (due to the electron distribution function)	+
Set by indirect estimates or calculated self-consistently	Plasma density distribution along the magnetic loop, n_e	+	+
	Ionization degree of chromosphere plasma in the loop, *x*	+ (due to the electron distribution function)	-
Fokker – Planck equation	Injection function: S(E, μ, s, t): δ, E_{start}, E_{end}, E_{break}, $S_1(s)$, $S_2(\alpha)$, $S_4(t)$ Albedo	+	+

FOKKER – PLANCK EQUATION

$$\frac{\partial f}{\partial t} = -c\beta\mu\frac{\partial f}{\partial s} +$$ Electrons transport

$$c\beta\frac{(1-\mu^2)}{2}\frac{\partial \ln(B)}{\partial s}\frac{\partial f}{\partial \mu} +$$ Magnetic mirroring

$$C_1\frac{c}{\lambda_0}\frac{\partial}{\partial E}\left(\frac{f}{\beta}\right) + C_2\frac{c}{\lambda_0\beta^3\gamma^2}\frac{\partial}{\partial \mu}\left[(1-\mu^2)\frac{\partial f}{\partial \mu}\right] +$$ Coulomb losses and diffusion

$$\frac{e\mathcal{E}\beta\mu}{m_e c}\frac{\partial f}{\partial \mathrm{E}} + \frac{e\mathcal{E}(1-\mu^2)}{m_e\beta c}\frac{\partial f}{\partial \mu} +$$ Self-induced electric field

$$\frac{1}{2}\left(\frac{\delta B}{B}\right)^2\frac{v}{\lambda_B}\frac{\partial}{\partial \mu}\left[|\mu|(1-\mu^2)\frac{\Omega_{ce}^2}{\Omega_{ce}^2 + (\mu v/\lambda_B)^2}\frac{\partial f}{\partial \mu}\right] +$$ Diffusion on magnetic field fluctuations

$$+S(E,\mu,s,t)$$ Source function

$$C_1 = x + \frac{1-x}{2}\frac{\ln\beta^2 g^2 E/\alpha_F^4}{\ln\Lambda}, \quad C_2 = \frac{1}{2} + \frac{1+g}{4}C_1$$

$$W(k_\parallel) = \frac{(\delta B)^2}{\pi}\frac{(1/\lambda_B)}{(1/\lambda_B)^2 + k_\parallel^2}$$ (Kontar et al., 2013)

$$\lambda_0(s) = \frac{10^{24}}{n(s)\ln\Lambda}, \beta = \frac{v}{c}, \mu = \cos\alpha, \gamma = E+1, E = \frac{E_e}{m_e c^2}$$

$$\mathcal{E}(s,t) = \frac{j(s,t)}{\sigma(s)} = \frac{e}{\sigma(s)}\int_{E_{min}}^{E_{max}} v(E)dE\int_{-1}^{1} f(t,s,E,\mu)\mu d\mu$$

$$\frac{1}{\sigma} = \frac{7.26\cdot10^{-9}}{x\cdot T_e^{1.5}}\ln\Lambda + \frac{7.6\cdot10^{-18}(1-x)T_e^{0.5}}{x}$$

$$k_\parallel = \Omega_{ce}/v|\mu|$$

$$\Omega_{ce} = eB/m_e\gamma c$$

$$C(z) \propto \exp(-z/\lambda_B)$$

$$z(t) = \mu v t$$

Parameters obtained from observations and used in modeling

RHESSI

- X-ray flux
- Energy X-ray spectra <130keV
- Space locations of the X-rays of 28-58, 70-130 keV
- Estimated volume of the HXR sources
- Estimated plasma density - SXR

Nobeyama Radioheliograph

- Relative source location 17 , 34 GHz
- 17/34 GHz source brightness ratio

MDI +GS simulator

- Magnetic field structure - LFFF

The DATA analyses:

HXR observations:

- Analysis of time dynamics of HXR sources.
- Association with specific magnetic field structures
- Obtaining restrictions on the HXR spectrum in the range up to ~ 130 keV taking into account the spread of values at a previously unknown albedo effect (OSPEX), plasma density distribution and degree of ionization in the chromosphere.

UV - radiation:

- Analysis of the loop structures

GS 17, 34 GGH:

- Estimation of the electron spectrum >200 keV in GX
- Analysis of time dynamics of GS sources
- Association with specific field structures
- Estimates of n_b, E_b, n_e (Razin effect) and self-absorption are carried out after the first kinetic test models

HXR and GS DATA SOL2002:11:10 T 03:05:13, M2.6

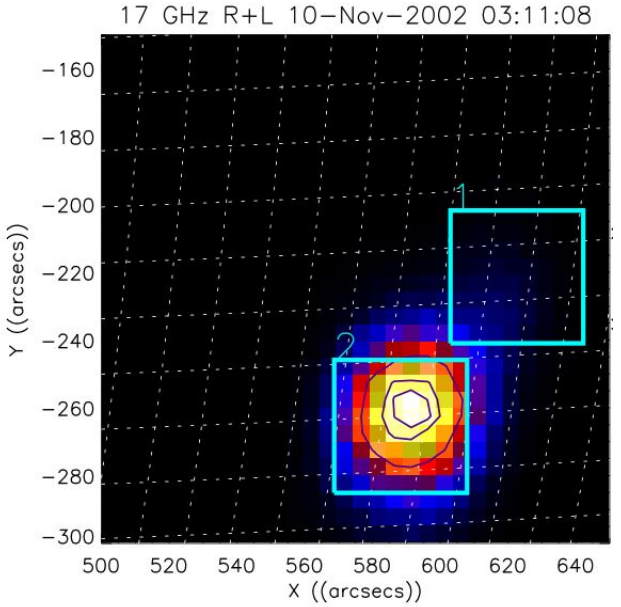

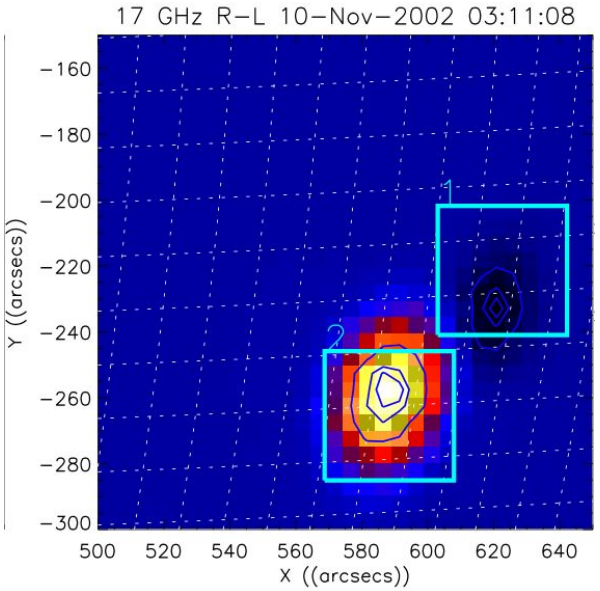

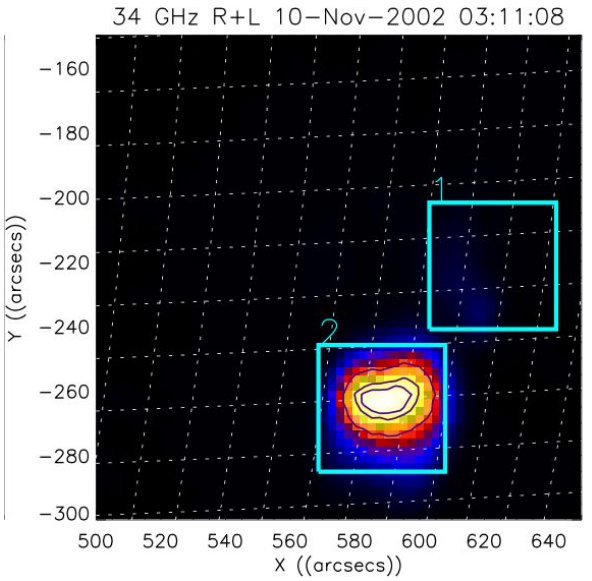

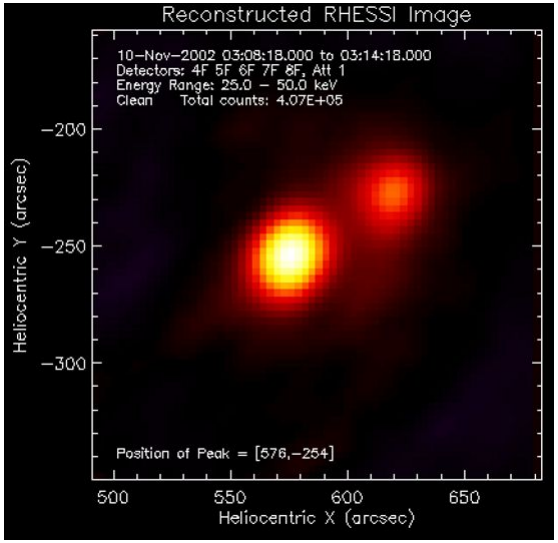

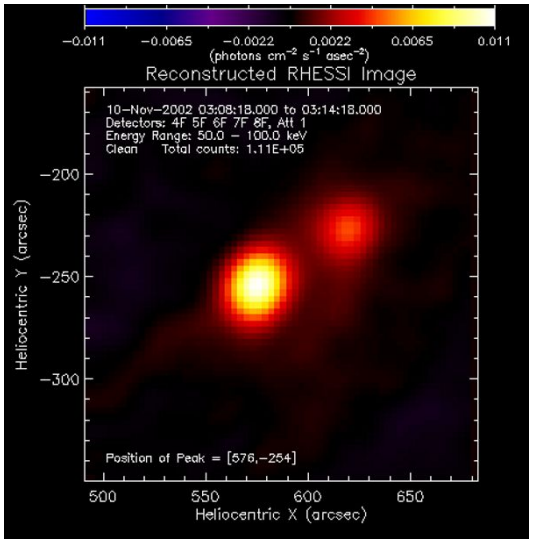

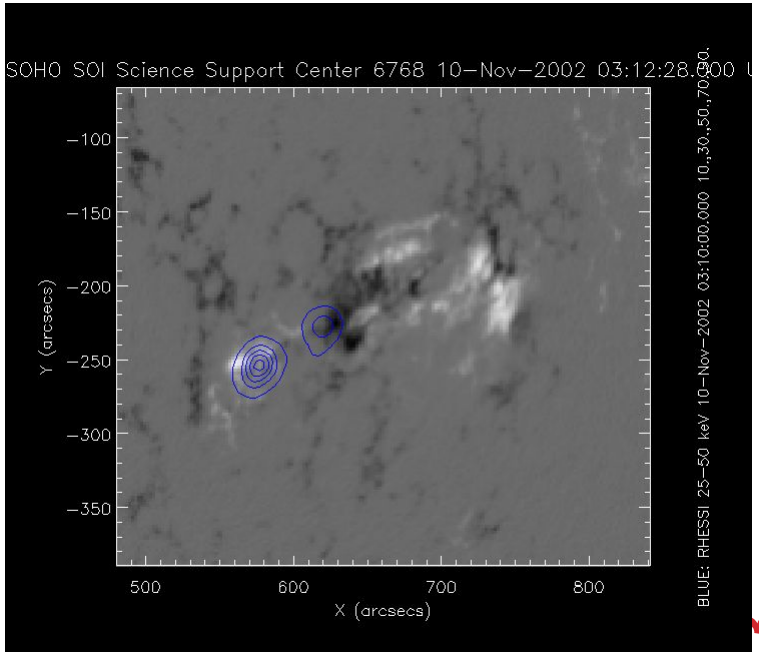

MAGNETIC FIELD

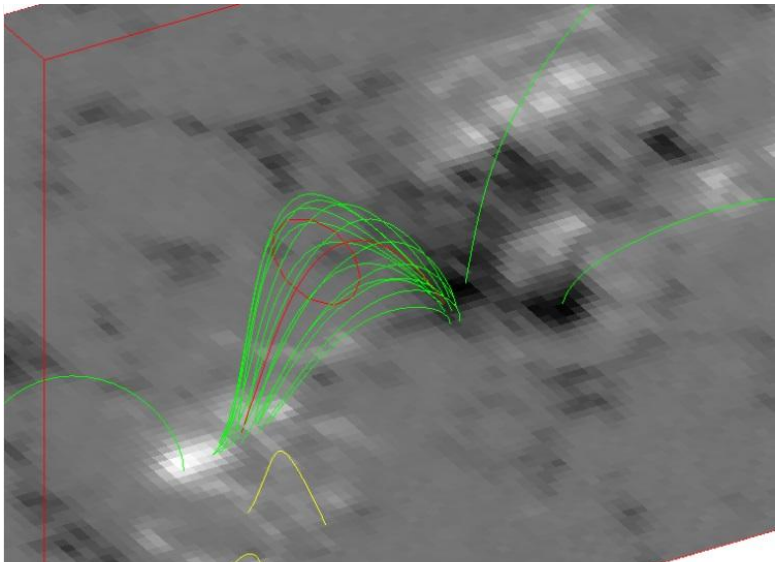

Plasma Density

$$n_e = 1.25 \cdot 10^{13} \left(z / 1\mathrm{Mm} \right)^{-2.5} \mathrm{cm}^{-3}$$

Aschwanden, M. J., Brown, J. C., and Kontar, E. P.: 2002, *Solar Physics* **210**, 383

n_{LT} = ~10^9 - increases up to ~10^{10} cm^{-3}

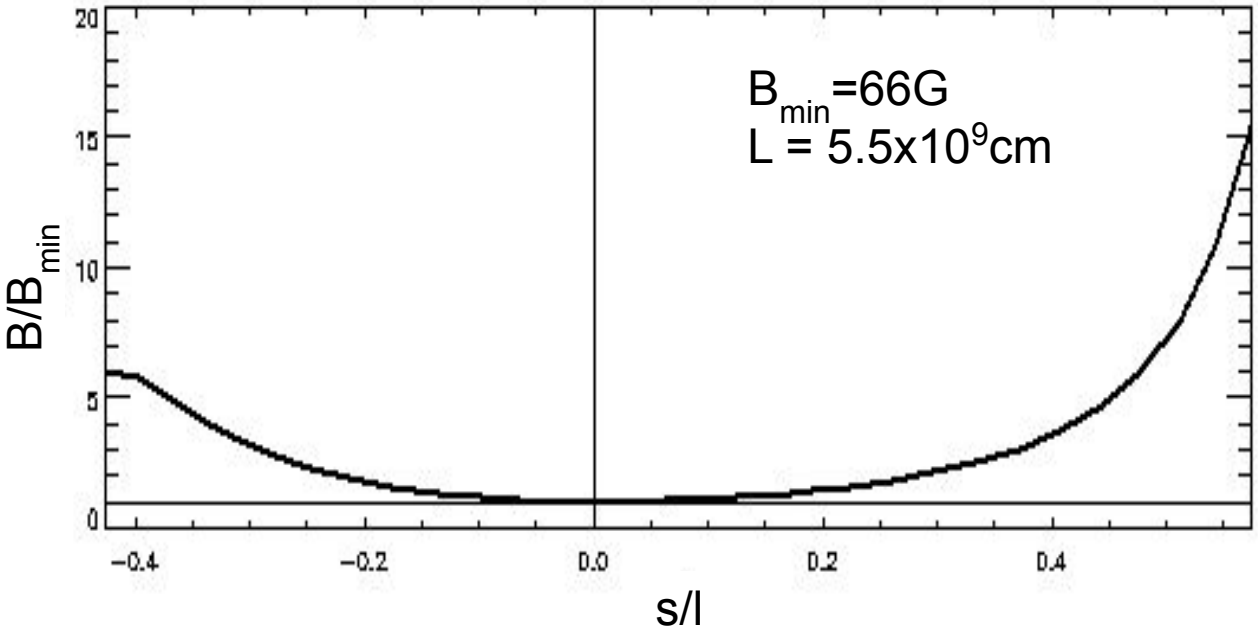

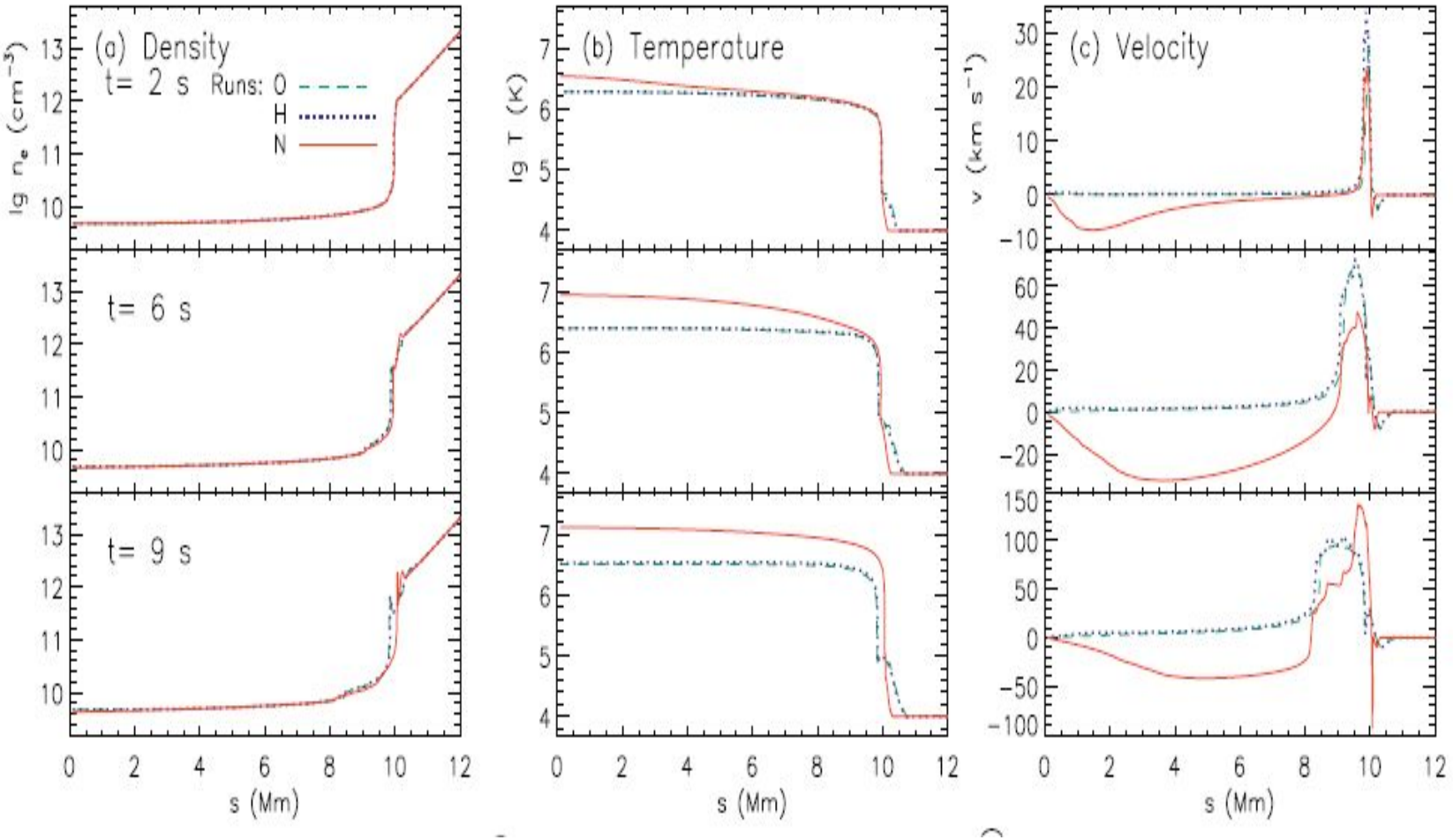

Liu W., Petrosian V., Mariska J.T. , 2009.

SOL2002:11:10 T 03:05:13, M2.6 Time History

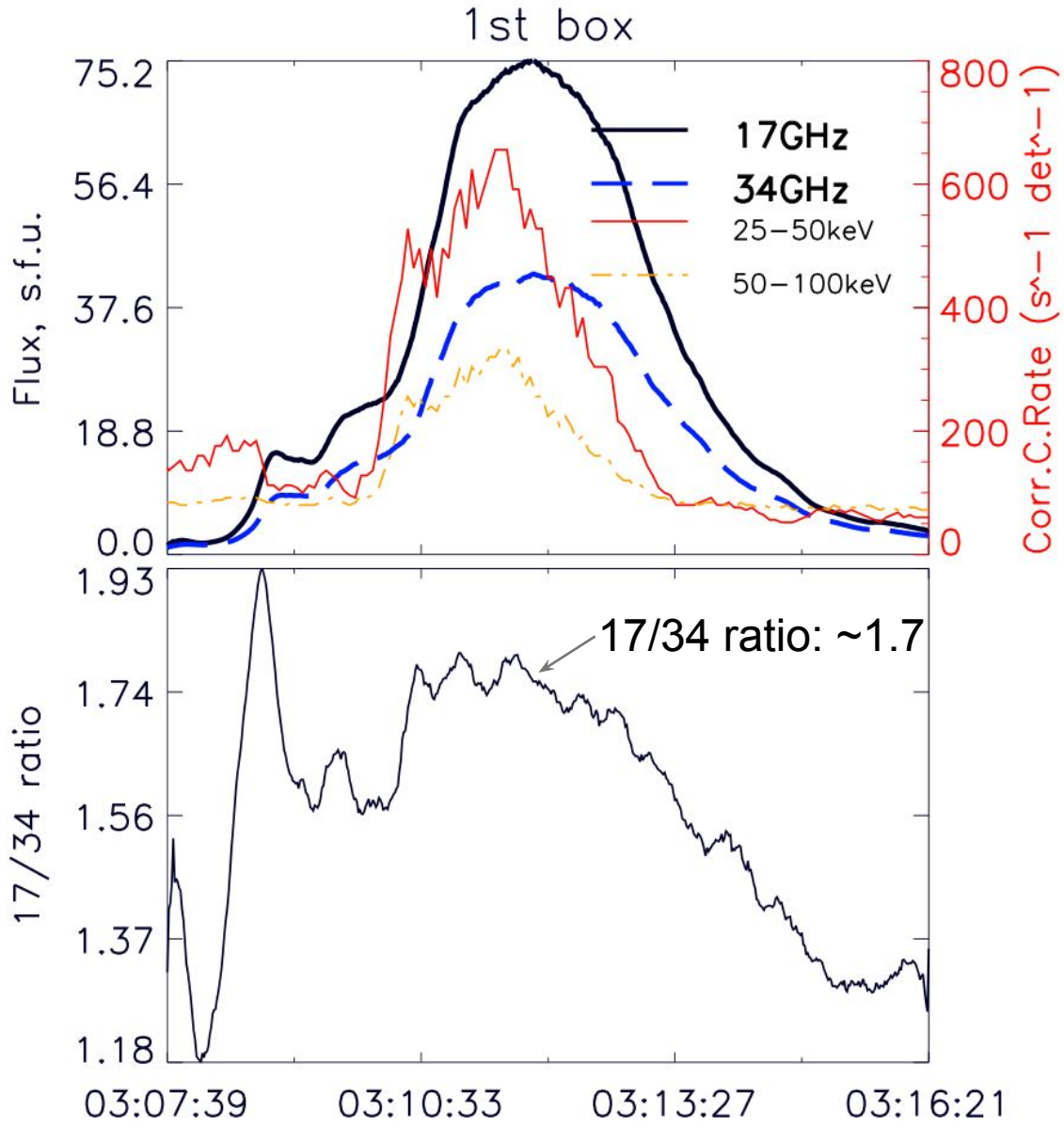

10 November
2002
03:11 UT
M2.6

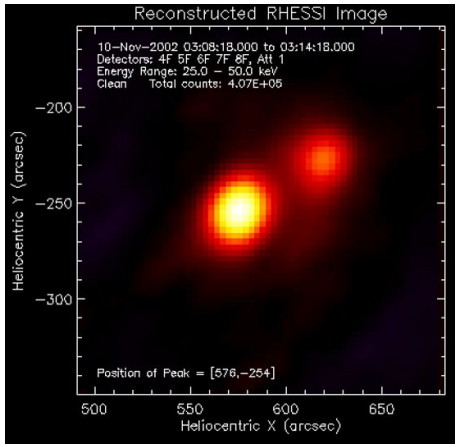

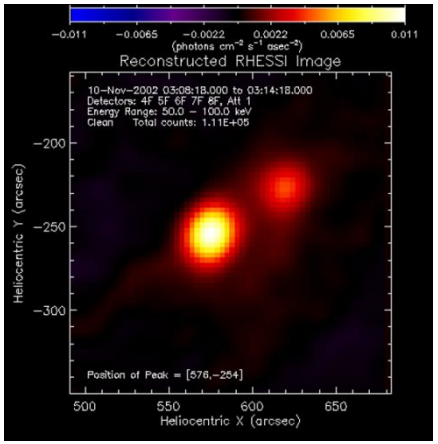

Ratio of X-Rays from two local sources

♦ Diamonds - simulated Flux ratio

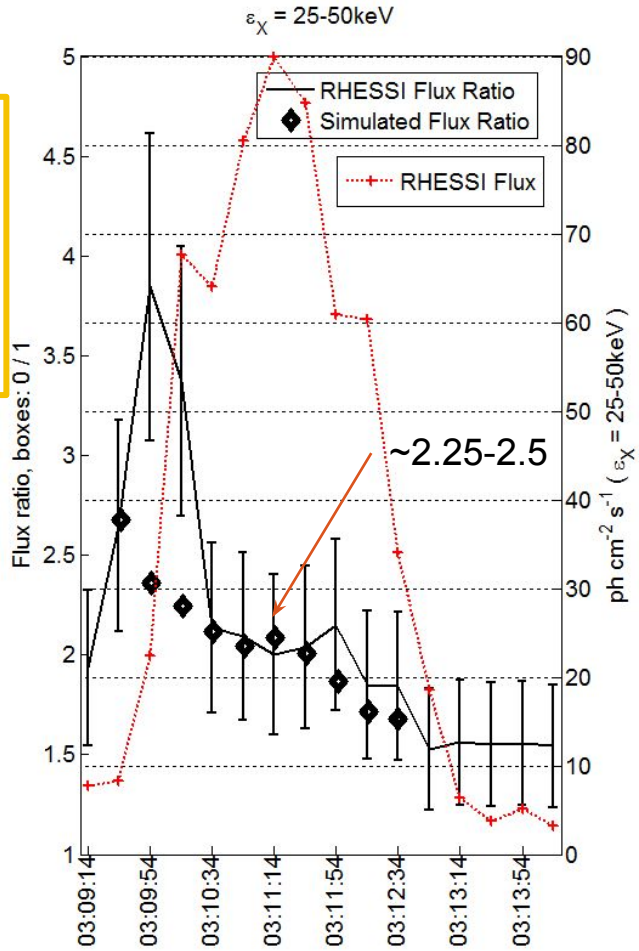

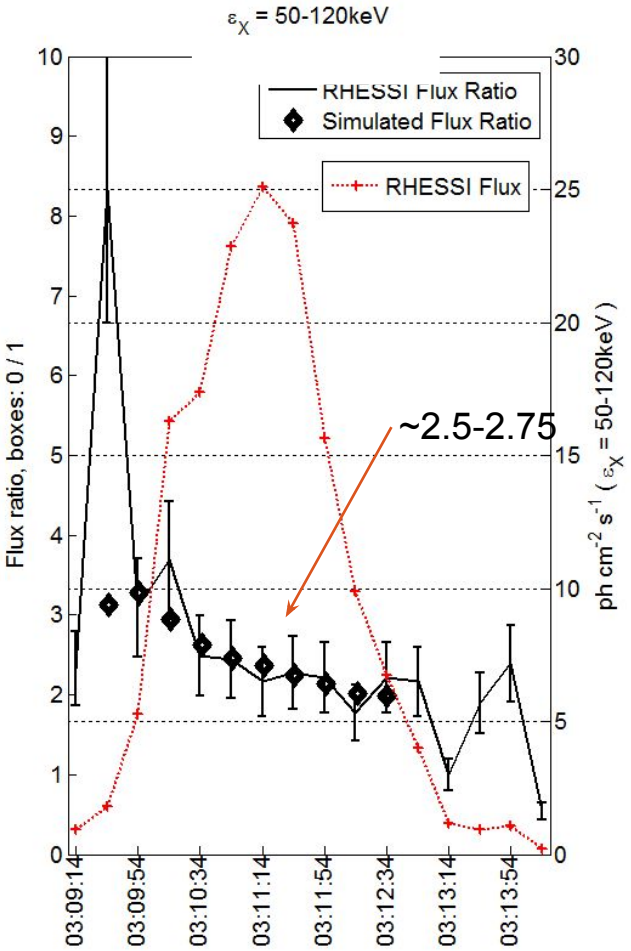

CONSIDERED TYPES OF MODELS IN THE SOURCE

SOURCE FUNCTION S(E,μ,s,t) **varied** (μ=cos(α)):

By angular distribution:

- Isotropic source
- Symmetric and asymmetric with varying degrees of anisotropy

By source localization: at the top, between the base and the top, and others.

By type of spectrum:

- 1 power law, broken power law
- consisting of two populations of electrons

By the presence of additional scattering mechanisms: magnetic fluctuations, ion-sound turbulence

The time profile for the source is taken from the 80-130 keV RHESSI data range

$S_2(\alpha)=$	1	isotropic
	$\cos^{2n}(\alpha)$	longitudinal
	$\sin^{2n}(\alpha)$	transverse
	$\exp\{-(\alpha-\alpha_1)^2/\alpha_0^2\}$	asymmetric

Finally, a model with parameters in a narrow range satisfied all observational criteria:

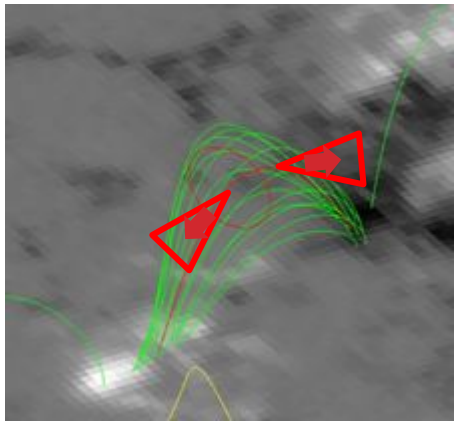

- Anisotropic source at the looptop $S(\alpha)=A(t)\exp\{-(\alpha-\alpha_1)^2/\alpha_0^2\}+$ $+B(t)\cos^8(\alpha)$, $\alpha_0=36^o$, $\alpha_1=90^o$
- Energy Dependence: Two Electron Populations

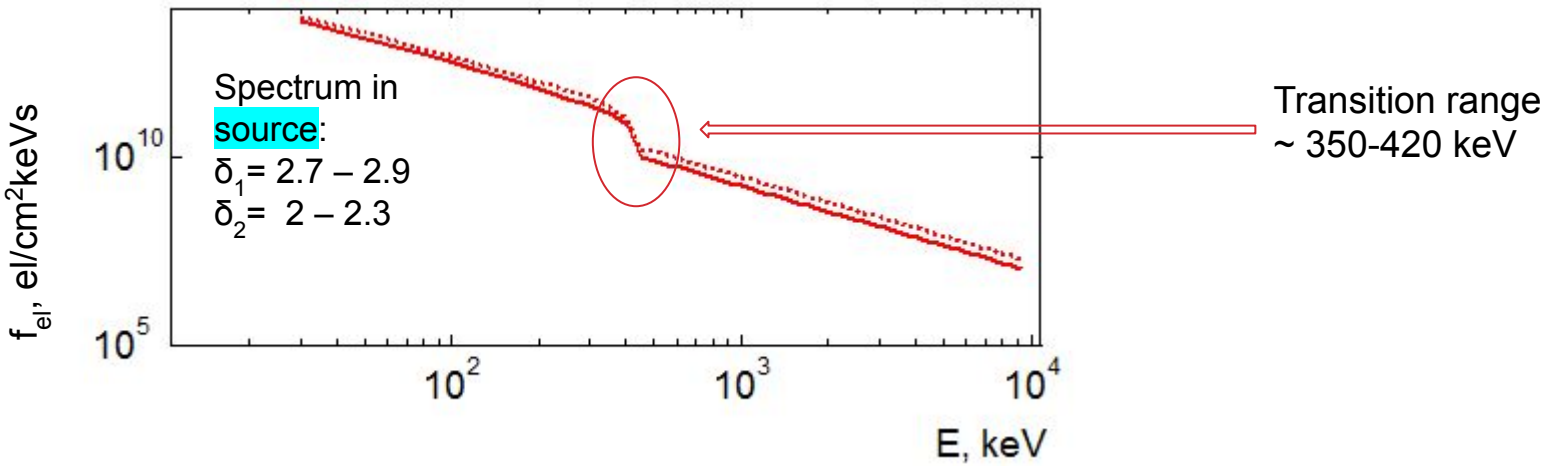

- The energy flux of accelerated electrons is 2×10^9 erg / cm^2s within an accuracy of ± 30% (the uncertainty is associated with the error in determining the loop volume)
- The level of magnetic fluctuations $\delta B/B << 10^{-2}$ at $\lambda_B = 10^7$ cm
- Energy density of ion-sound waves $W^s/n_e k_B T_e << 10^{-4}$

10 November 2002 03:11 UT M2.6

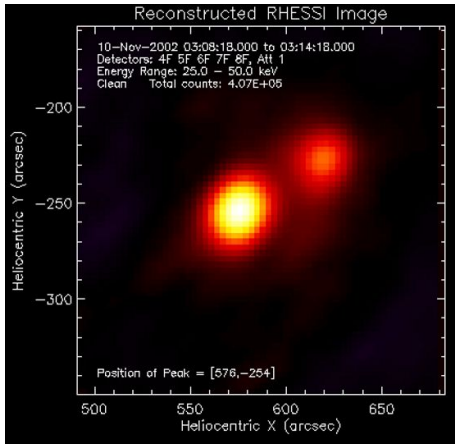

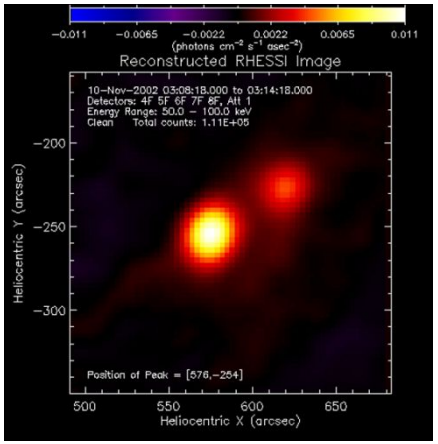

Ratio of X-Rays from two local sources

♦ Diamonds - simulated Flux ratio

$S(\alpha)=A(t)\exp(-(\alpha-\alpha_1)^2/\alpha_0^2)$, $\alpha_0=36^o$, $\alpha_1=90^o$ $+B(t)\cos^8(\alpha)$

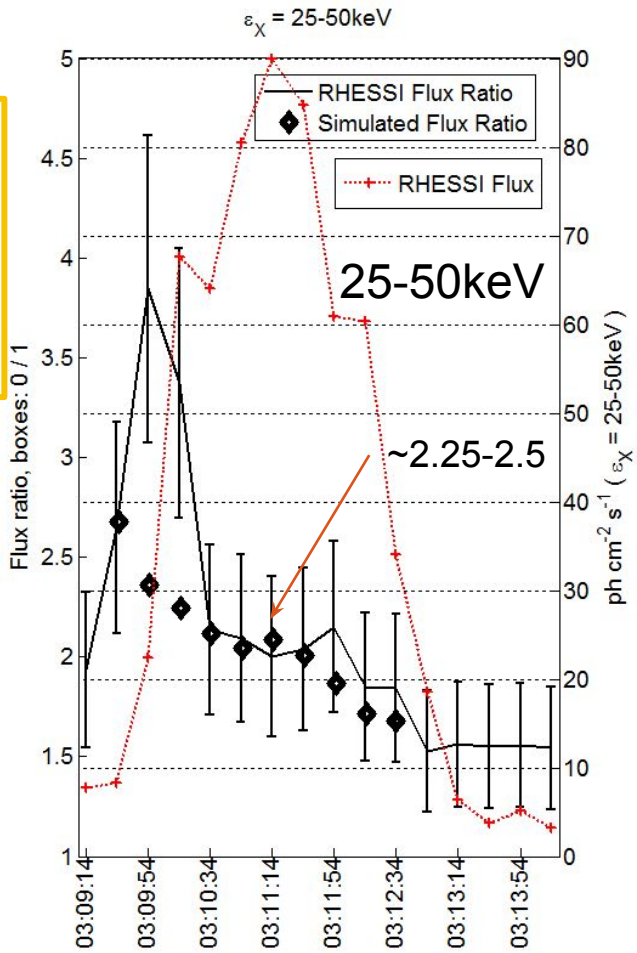

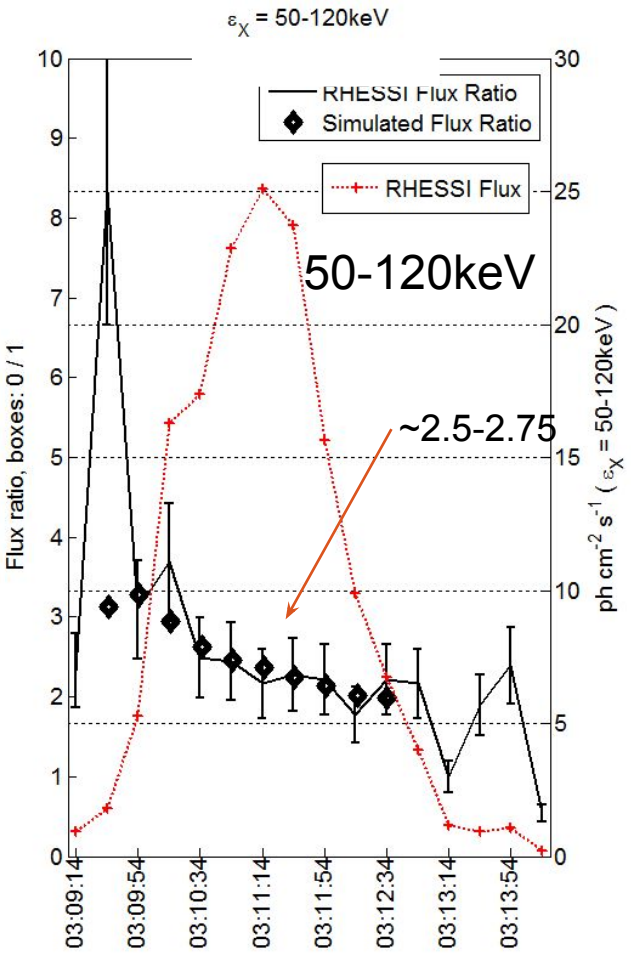

X-RAY MODELING RESULTS

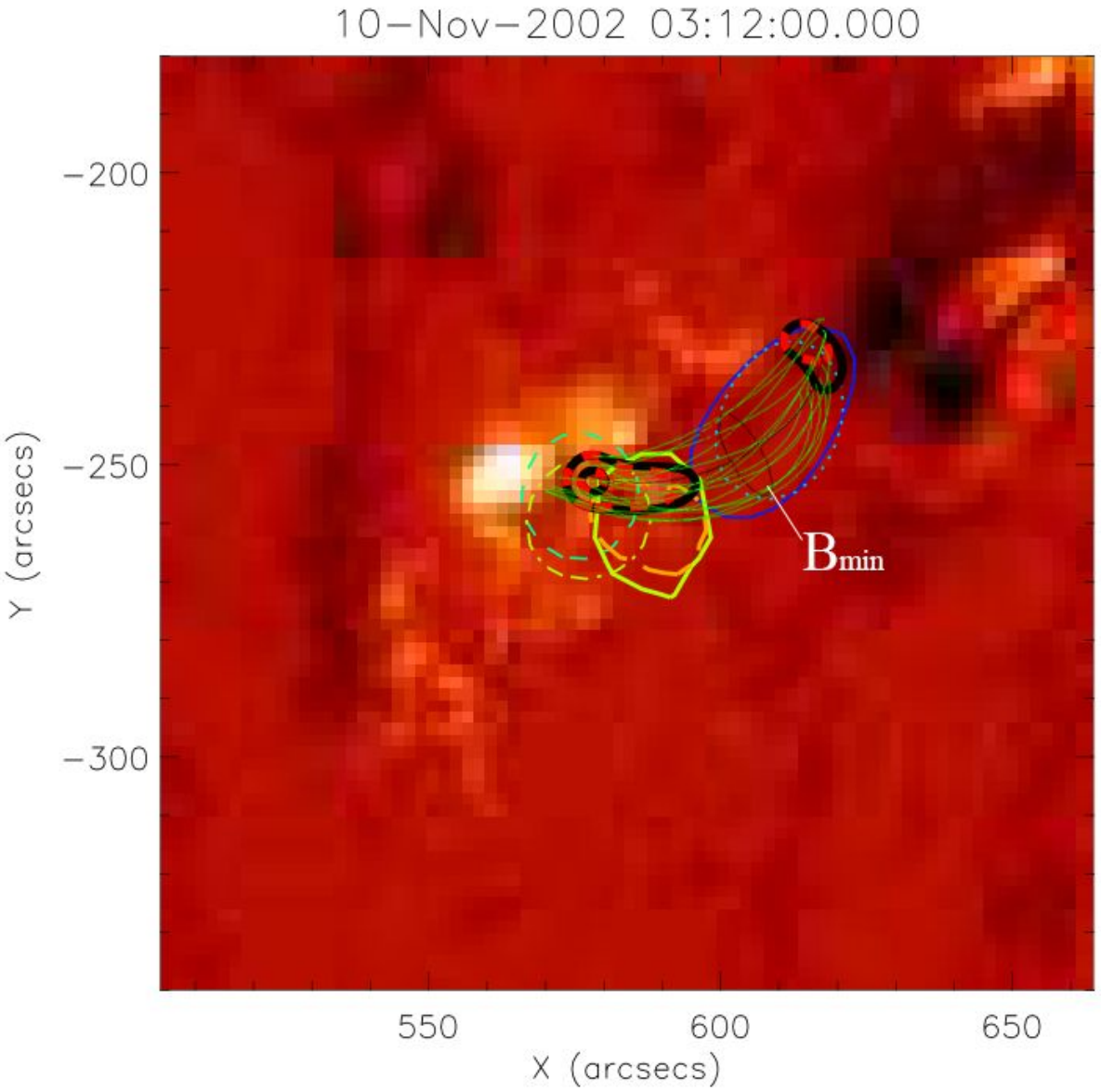

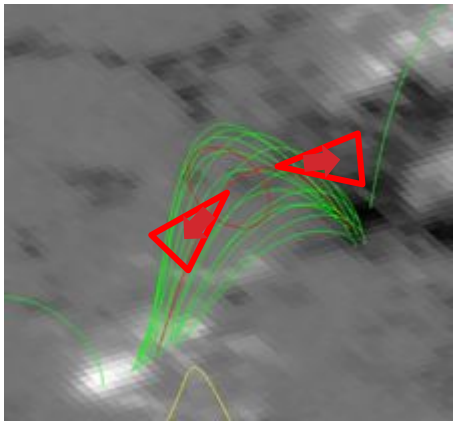

RHESSI 3.0−6.0 keV
RHESSI 6.0−12.0 keV
RHESSI 28.0−58.0 keV
RHESSI 70.0−130.0 keV
GS 17 GHz
GS 34 GHz
Sim.HXR 28−58 keV
Sim.HXR 70−130 keV

Conformed:

- HXR fluxes from each local source
- The ratio of the HXR fluxes in the southern and northern footpoints in each energy range

Gyrosynchrotron radiation. Simulation results

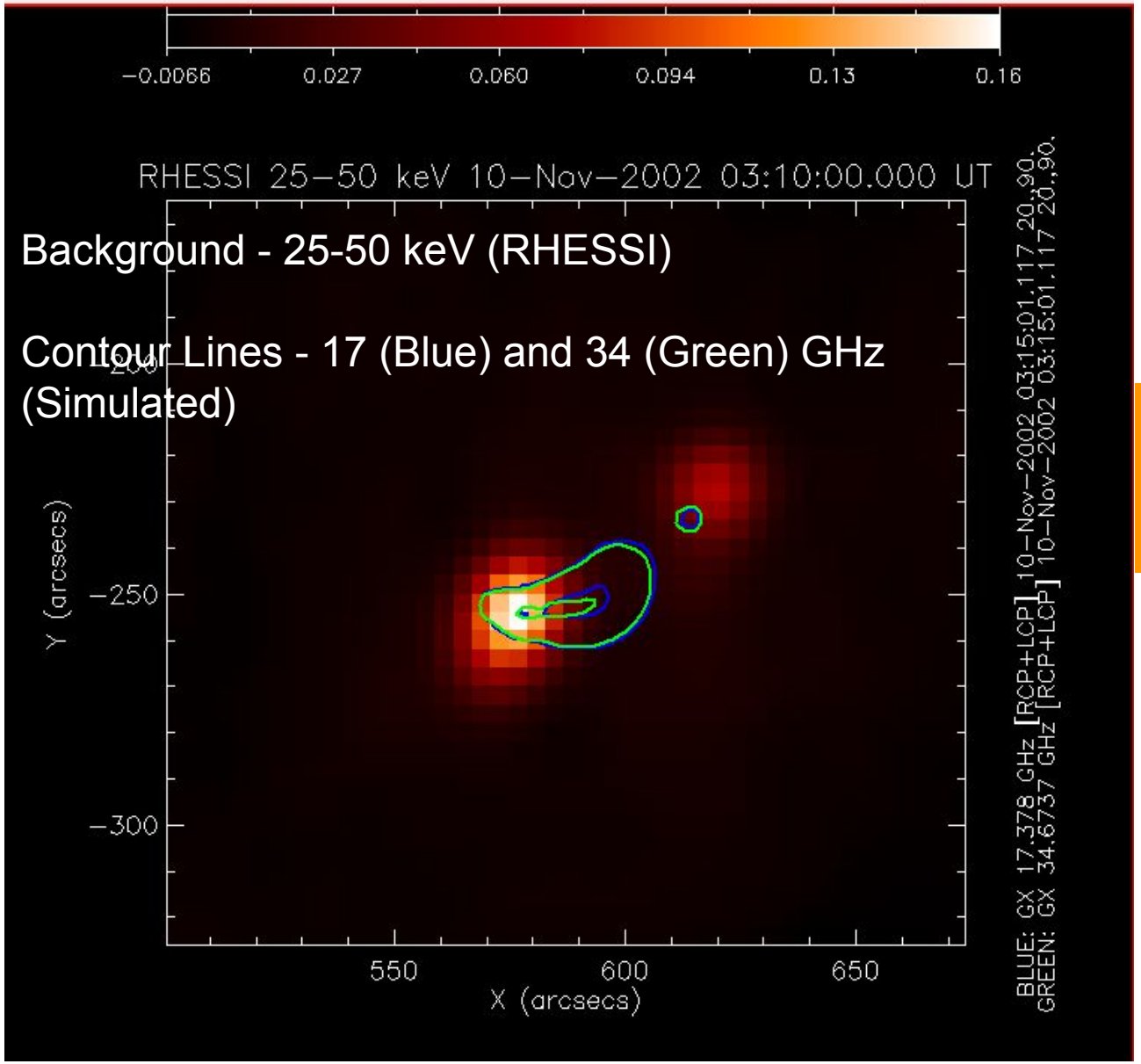

Conformed:

- 17 and 34GHz fluxes

RESULTS OF MODELING DYNAMIC CHARACTERISTICS: OBSERVED SOFT-HARD-SOFT PATTERN IN THE HXR SPECTRUM IN THE 28-58 keV

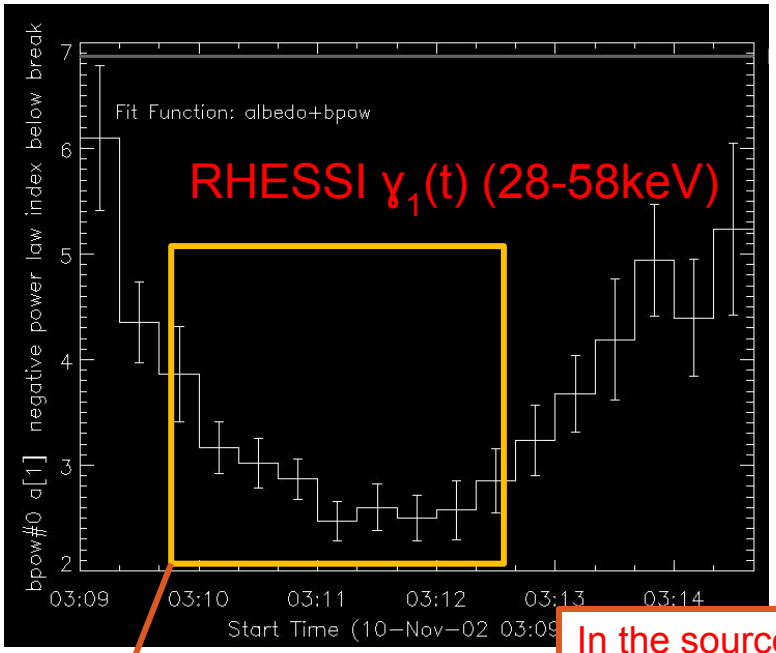

Simulation result $\gamma_1(t)$ (28-58keV)

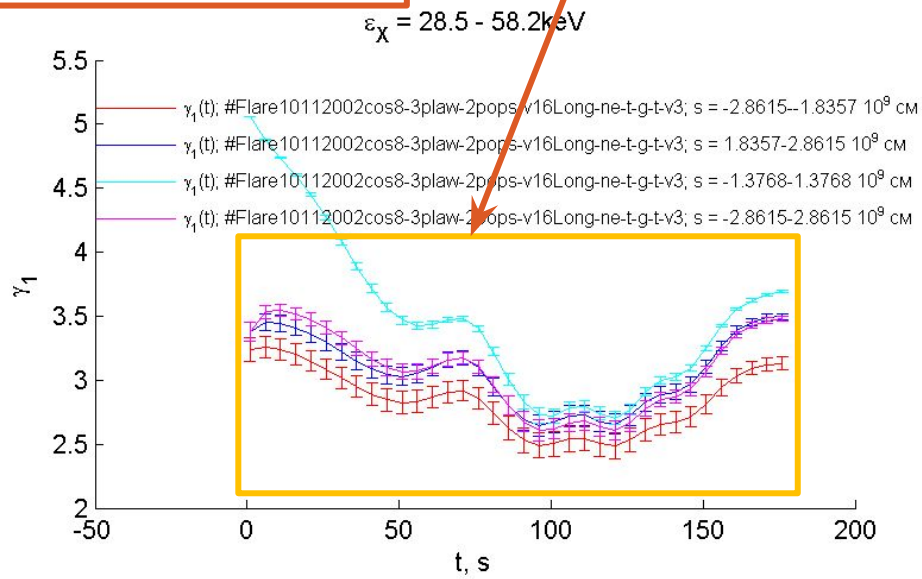

In the source $\gamma_1(t)$=4.5--2.8--4

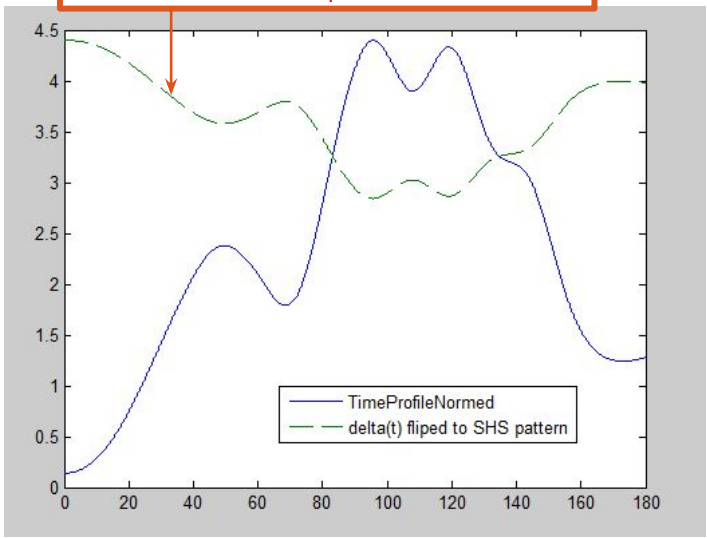

Electron distribution along the loop at the peak flux

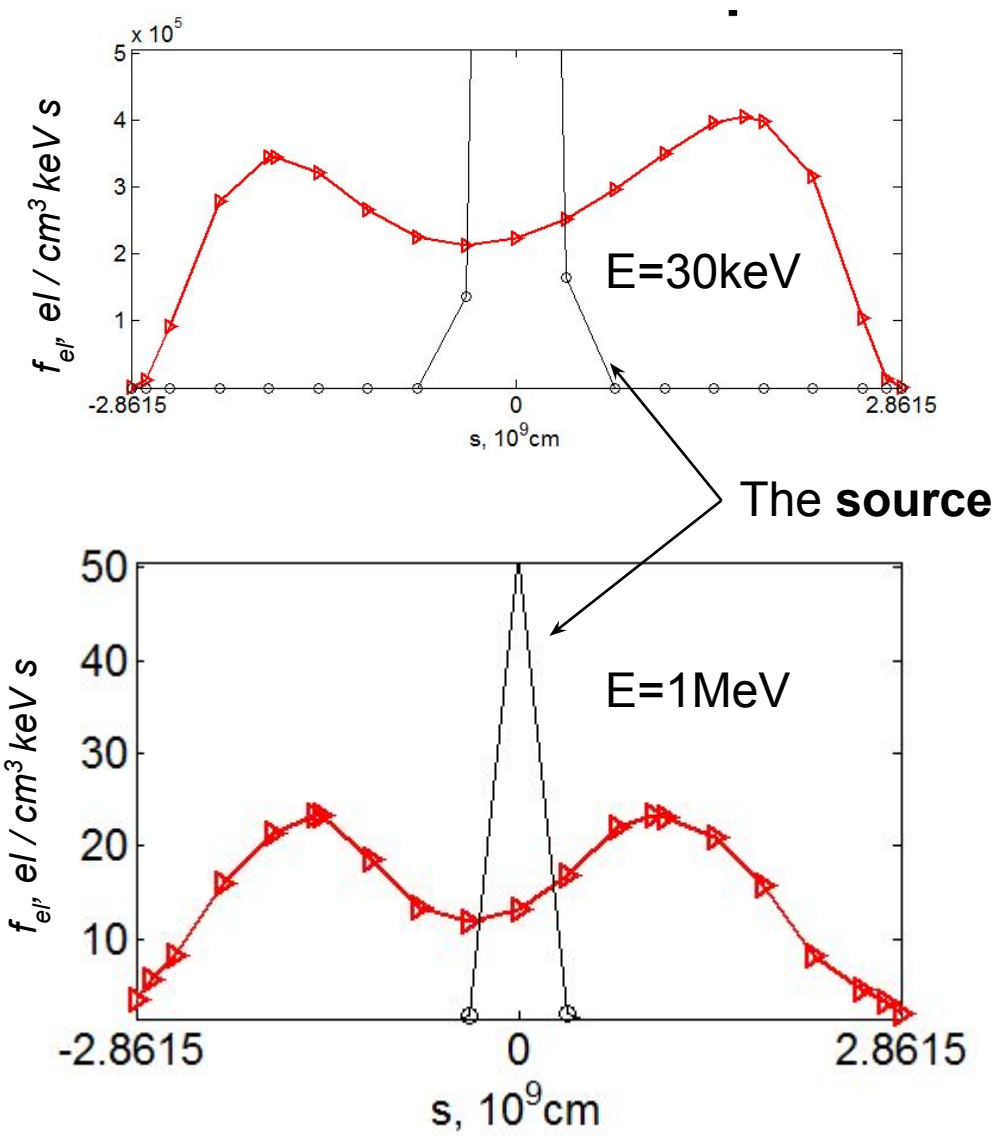

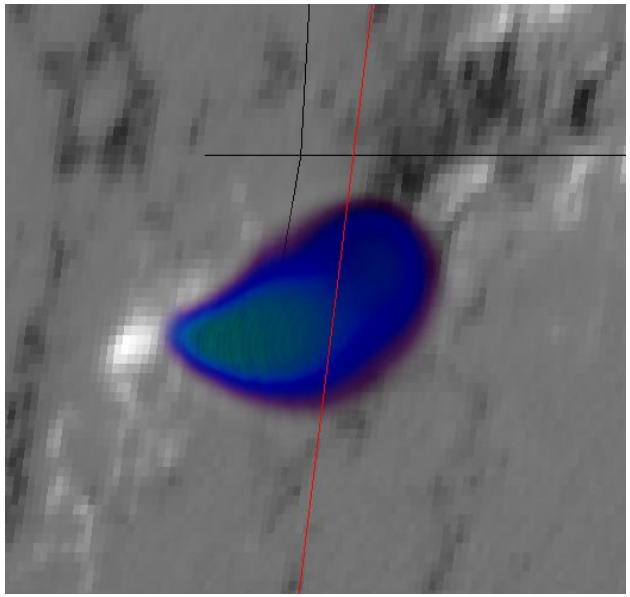

t=peak

Pitch-angle distribution of electrons in the legs at the peak of the flux

E=30keV

Source
$\cos^8(\alpha)$
$f_e/\max(f_e)$

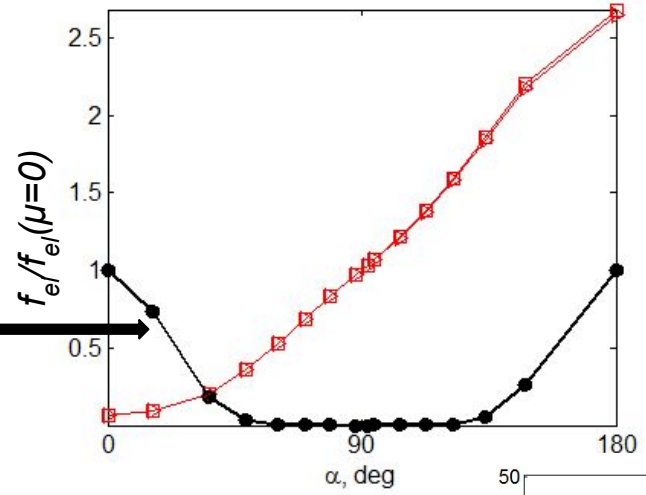

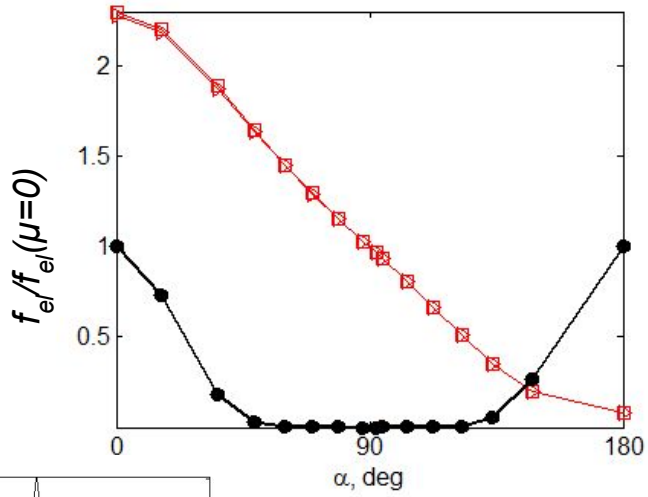

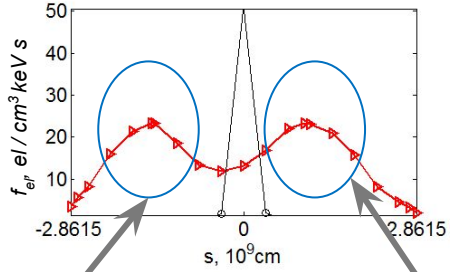

E=1MeV

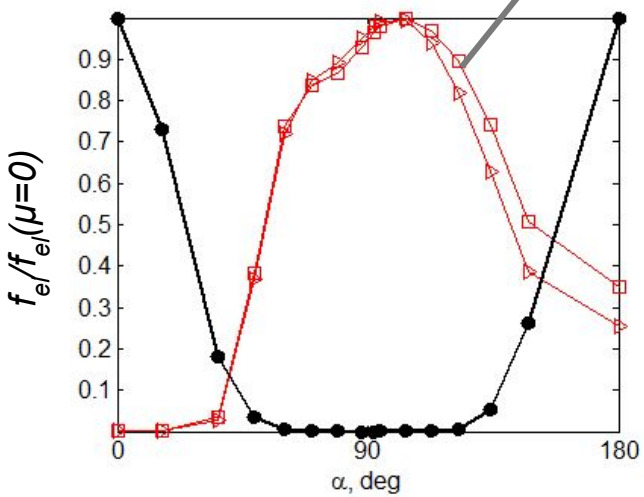

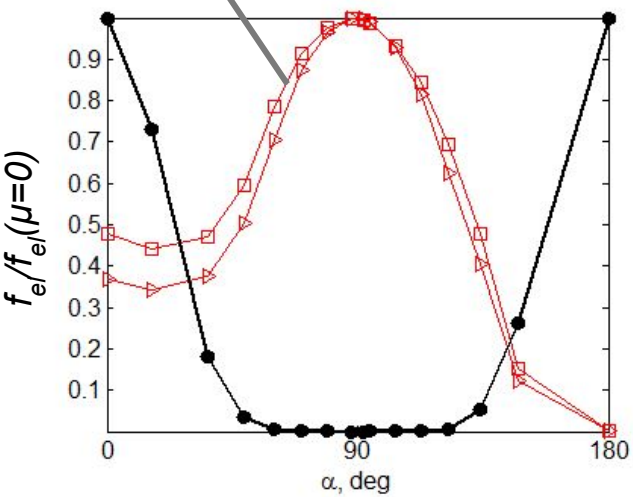

t=peak

Simulation results
SOL2002:11:10 T 03:11 M2.6

- Two Hard X-ray sources – Northern and Southern in opposite footpoints of the magnetic loop are distinctly allocated.
- Loop length - L ~ 5.5×10^9cm. The magnetic field is asymmetric, at the looptop is 66 G, in the southern footpoint - 400 G and 1000 G in the northern footpoint.
- The plasma density at the looptop is ~10^9 cm^{-3} in the initial flare phase and increases up to ~10^{10} cm^{-3} in the peak and decay phases as a result of the thermal plasma evaporation.
- Accelerated electrons injected near the looptop in the direction of the southern footpoint at the initial phase. The injection took place in the form of a Gaussian profile with a half-width (FWHM) of 2 Mm.
- The energy flux of the accelerated electrons at the peak ~$2\bullet10^9$ erg/cm^2s in the energy range of 30 keV – 10 MeV.

Simulation results SOL2002:11:10 T 03:11 M2.6

- At the injection site in the peak, the pitch angle distribution of accelerated electrons transformed to anisotropic $S_2(\alpha) = \cos^8(\alpha)$.
- The transition region E~350-420 keV is the region of a sharp change in the electron spectrum, separating them, in fact, into two populations. The energy spectral index of accelerated electrons up to the transition region δ_1 is variable, varying in time from 4.5 to 2.8 at the peak and up to 4 at the decay (SHS). At the peak, power-law index of the accelerated electrons after the transition region δ_2 = 2-2.3.
- The average number density of accelerated electrons, mainly responsible for radiation at 17 GHz and 34 GHz, is $n_b \sim 3\times10^3$ cm^{-3} (E > 350 keV).
- The average number density of the accelerated electrons in the range 30keV-10MeV n_b is ~10^7 cm^{-3} in the region of the radio source 17GHz and n_b ~$2\cdot10^5$ cm^{-3} in the Hard X-ray source in the southern part of the magnetic loop.